

# Spin- and momentum-correlated atom pairs mediated by photon exchange

Fabian Finger,<sup>1,\*</sup> Rodrigo Rosa-Medina,<sup>1,\*</sup> Nicola Reiter,<sup>1</sup>  
Panagiotis Christodoulou,<sup>1</sup> Tobias Donner,<sup>1,†</sup> and Tilman Esslinger<sup>1</sup>

<sup>1</sup>*Institute for Quantum Electronics, ETH Zürich, 8093 Zürich, Switzerland*

(Dated: March 20, 2023)

Pairs of correlated particles are at the core of complex many-body phenomena and their control is essential for quantum technologies. Engineering pairs that are simultaneously correlated in their external and internal degrees of freedom is a major challenge. In this work, we experimentally demonstrate a mechanism for generating pairs of atoms in well-defined spin and momentum modes. This mechanism couples atoms from a degenerate Bose gas via a superradiant photon-exchange process mediated by the vacuum mode of an optical cavity. The scheme is independent of collisional interactions, fast and tunable. We observe a collectively enhanced production of pairs, characterize their statistics, and measure inter-spin correlations in momentum space. Our observation of coherent many-body oscillations involving well-defined momentum modes offers promising prospects for quantum-enhanced interferometry using entangled matter waves.

Mechanisms generating correlated pairs of particles have proven pivotal in diverse fields of physics. In cosmology, vacuum fluctuations are at the origin of the creation of elementary particle-antiparticle pairs and Hawking radiation [1, 2]. In condensed-matter systems, the pairing of quasiparticles drives strongly correlated phenomena, such as phonon-mediated superconductivity [3] or vortex-induced superfluidity [4]. In quantum-optics experiments, entangled photons are produced through parametric down-conversion, with high-potential applications in metrology and quantum information science [5]. Similar approaches have been explored with ultracold atomic gases to correlate massive particles either in their internal [6–12] or motional [13–25] degrees of freedom. Quantum metrology based on atom interferometry, including precision gravimetry and magnetometry [26, 27], would benefit from a rapid pair production in well-defined momentum modes. However, existing schemes relying on collisions are limited by the timescales of contact interactions.

Fast timescales are characteristic for strong light-matter interactions and photon-atom pairs can be created in superradiant processes [28]. Yet, pairs comprising different species are difficult to manipulate and detect. To overcome this, strong light-matter coupling can be used as a building block to correlate matter pairs. This had been demonstrated with Rydberg atoms exchanging a photon in a microwave cavity [29] and has more recently been extended to generate matter pairs and control spin correlations in thermal atomic ensembles [30–32].

Here, we employ a Bose-Einstein condensate (BEC) coupled to a high-finesse optical cavity to generate photon-mediated atom pairs correlated simultaneously in their spin and momentum. Unlike schemes relying on isotropic collisions [12, 33], our implementation directly couples individual momentum modes, offering an efficient route for pair production with large mode occupation. The fast timescales associated with the strong light-matter coupling are on the order of tens of microsec-

onds and allow us to separate this process from typical dissipative mechanisms in atomic systems, such as heating, three-body losses, and trapping effects [34, 35]. We explore the properties of the pairs by examining their statistics and inter-spin correlations in momentum space. Our scheme enables independent control over unitary and additional dissipative processes which originate from the open character of our system [36, 37], allowing us to observe coherent many-body oscillations.

In our experiments, we prepare a <sup>87</sup>Rb BEC consisting of up to  $N \approx 8 \times 10^4$  atoms in the  $m = 0$  magnetic sublevel of the  $F = 1$  hyperfine manifold. We couple the atoms dispersively to a single mode of a high-finesse optical cavity by illuminating them with a running-wave laser drive propagating along the  $z$  direction, cf. Fig. 1a. The drive has a wavelength  $2\pi/k$  and is switched on for a quench time  $t$ . This coupling converts atoms in  $m = 0$  with zero momentum into pairs of  $m = \pm 1$  with opposite recoil momenta  $\hbar k$  along  $z$ . The atoms additionally acquire momentum  $\hbar k$  symmetrically in  $\pm x$  direction following the standing-wave structure of the cavity mode. This process conserves both the total center of mass and angular momentum of the atoms. The underlying coupling mechanism is a superradiant photon-exchange process involving the drive and the vacuum mode of the cavity field [30], as illustrated in Fig. 1a (upper panel). During this process, one atom in the mode  $|k_z = 0\rangle_{m=0} \equiv |0\rangle_0$  scatters a photon from the drive and flips its spin to either  $m = \pm 1$  while obtaining a recoil momentum  $\hbar k$  along  $+z$  and populating the modes  $|+k\rangle_{\pm 1}$ . The emitted ‘virtual’ cavity photon is rescattered into the drive field by a second atom in  $|0\rangle_0$ , which obtains a recoil momentum along  $-z$  and populates the complementary spin state  $m = \mp 1$ , i.e., the modes  $| -k\rangle_{\mp 1}$ . Pair production can occur via two discernible channels with coupling rates  $\chi_+$  and  $\chi_-$ , depending on the first atom occupying the mode  $|+k\rangle_{+1}$  or  $|+k\rangle_{-1}$ , cf. Fig. 1a (lower panel); for similar rates, the generated pair is expected to occupy a balanced super-

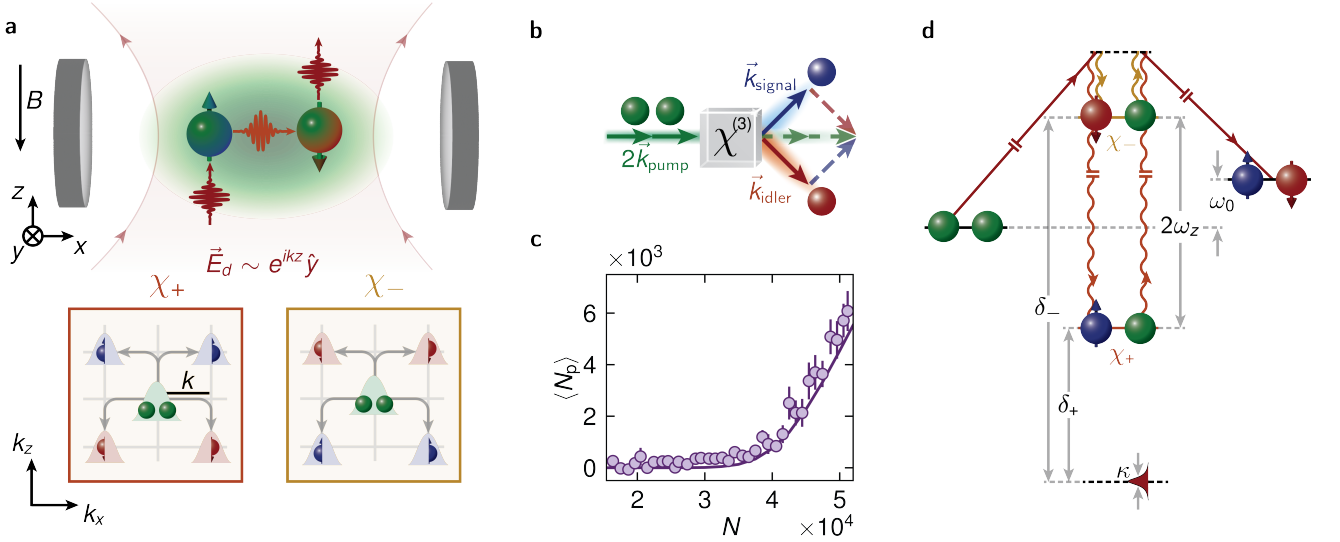


FIG. 1. **Spin-momentum pairs in an optical cavity.** **a**, Upper panel: A BEC inside a cavity is illuminated by a running-wave drive, with the magnetic field  $B$  defining the quantization axis. An  $m = 0$  atom (green) flips its spin to  $m = 1$  (blue) while scattering a photon into the cavity mode. This photon is rescattered by a second  $m = 0$  atom, changing its state to  $m = -1$  (red), and resulting in an atom pair with opposite spin and momentum. Lower panel: Pair creation in momentum space via two channels  $\chi_{\pm}$ , depending on the first atom changing its spin to  $m = \pm 1$  (grid in units of recoil  $k$ ). **b**, Schematics of an optical parametric amplifier, with two pump photons (green) being converted into a pair of signal (blue) and idler (red) photons via the nonlinear interaction  $\chi^{(3)}$ . **c**, Experimentally observed mean number of pairs  $\langle N_p \rangle$  showing a super-linear growth with the initial atom number  $N$ . Throughout this work, the errorbars are the SE obtained via jackknife resampling. The solid line shows our numerical simulations; see Methods also for experimental parameters. **d**, Energy-level diagram describing our pair-production mechanism which is composed of two superradiant processes, each involving a drive (straight) and a cavity (curly arrows) photon. The intermediate modes are split by twice the linear Zeeman shift  $\omega_z$  and determine two discernible channels with coupling rates  $\chi_{\pm}$ , depending on the detunings  $\delta_{\pm}$  and the cavity loss rate  $\kappa$ . The offset  $\omega_0$  is set by the kinetic and internal energy of the pairs.

position of the modes associated with the two channels.

For initially unpopulated  $|+k\rangle_{\pm 1}$  and  $| -k\rangle_{\mp 1}$  modes, our mechanism amplifies vacuum fluctuations analogously to optical  $\chi^{(3)}$  parametric amplifiers [5], see scheme in Fig. 1b. The atoms in  $|0\rangle_0$  correspond to the input ‘pump’ mode, whereas the finite-momentum atom pairs in  $m = \pm 1$  compare with the output ‘signal’ and ‘idler’ modes. Experimentally, we observe a super-linear increase of the mean pair number  $\langle N_p \rangle$  when adjusting  $N$  for a fixed  $t = 65 \mu\text{s}$  (Fig. 1c). This behaviour is due to collective enhancement of the pair production, which results in coupling rates  $N\chi_{\pm}$  akin to the third-order susceptibility  $\chi^{(3)}$ . The timescale of this process is orders of magnitude faster than realizations relying on collisional spin-mixing dynamics ( $\sim 10 \text{ ms} - 1 \text{ s}$ ) [26].

To characterize the key properties of our system, we derive an effective many-body Hamiltonian  $\hat{H}$  using a few-mode expansion in spin and momentum space and adiabatically eliminating the cavity field. We obtain  $\hat{H} = \hat{H}_0 + \hat{H}_+ + \hat{H}_-$ , with approximate contributions

$$\hat{H}_0 = \frac{\hbar\omega_0}{2} \sum_{\vec{k}=\pm k} \left( \hat{c}_{\vec{k},1}^\dagger \hat{c}_{\vec{k},1} + \hat{c}_{-\vec{k},-1}^\dagger \hat{c}_{-\vec{k},-1} \right), \quad (1)$$

$$\hat{H}_{\pm} = \hbar\chi_{\pm} \left( 2\hat{c}_{-k,\mp 1}^\dagger \hat{c}_{+k,\pm 1} \hat{c}_{0,0} \hat{c}_{0,0} + \text{h.c.} \right), \quad (2)$$

where the bosonic operators  $\hat{c}_{\vec{k},m}^\dagger$  create atoms in the modes  $|\vec{k}\rangle_m$  with  $\vec{k} = \{0, +k, -k\}$  and  $m = \{0, +1, -1\}$  (Methods). The various energy scales of the system are schematically depicted in Fig. 1d. The first term,  $\hat{H}_0$ , describes the energy cost  $\hbar\omega_0 = 2\hbar q + 4\hbar\omega_{\text{rec}}$  for creating a single pair, with the quadratic Zeeman splitting  $q$  and the recoil kinetic energy  $\hbar\omega_{\text{rec}} = h \times 3.68 \text{ kHz}$ . The interaction terms,  $\hat{H}_{\pm}$ , describe the two discernible pair-production channels with the corresponding intermediate states being separated by twice the linear Zeeman splitting  $\omega_z$ . The coupling rates  $\chi_{\pm} = \eta^2 \delta_{\pm} / (\delta_{\pm}^2 + \kappa^2)$  depend on the decay rate of the cavity field,  $\kappa = 2\pi \times 1.25 \text{ MHz}$ , and the tunable parameters  $\eta$  and  $\delta_{\pm} = \omega_c - \omega_{\pm}$ ; here  $\eta$  denotes the two-photon scattering rate [38],  $\omega_c$  is the cavity resonance and  $\omega_{\pm}$  are the frequencies of the virtual cavity photons for the two channels.

The behaviour of our system is determined by the competition between  $\hat{H}_0$  and  $\hat{H}_{\pm}$ . For sufficiently strong negative couplings  $\chi_{\pm}$ , we expect finite pair occupation in the corresponding modes. In our system, the typical interaction time required to produce pairs,  $T_{\text{int}} = 2\pi / (N\chi_{\pm}) \approx 40 \mu\text{s}$ , is significantly shorter than the lifetime of the emergent matter waves, which separate from the  $m = 0$  BEC within  $T_{\text{LT}} \approx 1 \text{ ms}$  due to their finite

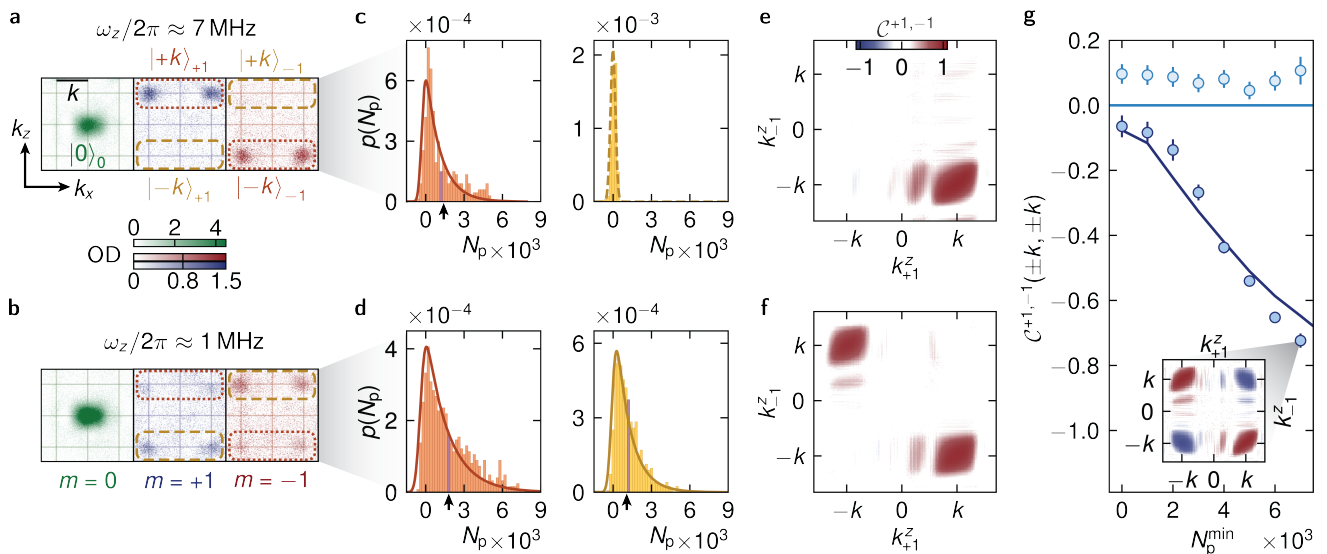


FIG. 2. **Pair statistics and correlations.** **a, b**, Exemplary spin-resolved momentum distributions for the single-channel (a) and double-channel (b) configuration. The orange and yellow boxes indicate the modes  $|\pm k\rangle_{\pm 1}$  and  $|\pm k\rangle_{\mp 1}$ , respectively. **c, d**, Pair statistics, generated through the  $\chi_+$  (orange) and  $\chi_-$  (yellow histograms) process, for the single-channel (c) and two-channel (d) configurations. The solid lines correspond to Bose-Einstein distributions with experimentally determined mean  $\langle N_p \rangle$  (purple coloured bin) convolved with our Gaussian detection noise (Methods). The arrows indicate the standard deviation of the resulting distributions, demonstrating  $\langle N_p \rangle \approx \sigma(N_p)$ . The dashed line is consistent with a distribution with zero mean pairs. **e, f**, Momentum space inter-spin correlation maps  $\mathcal{C}^{+1,-1}(k_{+1}^z, k_{-1}^z)$  for the single-channel (e) and two-channel (f) configuration, demonstrating the correlated nature of the produced pairs. We attribute the side patterns beside the correlation peaks to residual density-dependent imaging artifacts. **g**, Anticorrelation peaks  $\mathcal{C}^{+1,-1}(\pm k, \pm k) = [\mathcal{C}^{+1,-1}(k, k) + \mathcal{C}^{+1,-1}(-k, -k)]/2$  for realizations with  $N_p > N_p^{\min}$  for a single-channel (light blue) and two-channel (dark blue) configuration, with the solid lines showing the results from our numerical simulations. The anticorrelations increase with  $N_p^{\min}$  due to pump-mode depletion. The inset displays a representative correlation map for  $N_p^{\min} = 7 \times 10^3$ . See Methods for relevant experimental parameters.

momenta (Methods). This separation of timescales in our system,  $T_{\text{int}} \ll T_{\text{LT}}$ , ensures that pair production occurs deeply in the collective regime, and results in the occupation of well-defined individual momentum modes.

In the experiment, we individually control the couplings  $\chi_{\pm}$  by varying  $\delta_{\pm}$  via the combined tuning of  $\omega_c$  and  $\omega_z$ , and determine the populations of the various modes by measuring spin-resolved momentum distributions. For the relevant case of  $\delta_{\pm} < 0$ , and for sufficiently large  $\omega_z$ , only the  $\chi_+$  channel contributes and gives rise to pairs occupying the modes  $|+k\rangle_{+1}$  and  $|-k\rangle_{-1}$ . This is highlighted in the exemplary momentum distribution in Fig. 2a for  $\omega_z = 2\pi \times 7.09(1)$  MHz. For smaller  $\omega_z$ , both channels become active, resulting in concurrent occupation of the modes  $|+k\rangle_{-1}$  and  $|-k\rangle_{+1}$ , as shown in Fig. 2b for  $\omega_z = 2\pi \times 1.01(1)$  MHz. In the following, we make extensive use of these two settings, which we refer to as the single- and two-channel configurations, respectively.

By accumulating hundreds of experimental realizations for the single-channel (Fig. 2c) and two-channel (Fig. 2d) configurations, we obtain the respective pair statistics. The number of pairs associated with the  $\chi_+$  and  $\chi_-$  processes are shown in the left and right panels, respectively. When a channel becomes active, we observe large fluctuations compatible with a Bose-Einstein distribution

$p(N_p) = \langle N_p \rangle^{N_p} / (1 + \langle N_p \rangle)^{\langle N_p \rangle + 1}$  [11], which satisfies  $\sigma(N_p) = \langle N_p \rangle$  for the standard deviation  $\sigma(N_p)$  and the mean  $\langle N_p \rangle$  (see also arrow and purple bin in Figs. 2c and d). In the single-channel case, our observations are consistent with the system occupying a so-called ‘two-mode squeezed vacuum’ state, i.e., a superposition of twin-Fock states comprising  $|+k\rangle_{+1}$  and  $|-k\rangle_{-1}$  [39]. Multimode parametric amplification is not expected to alter the resulting distributions for an undepleted pump mode as long as the different channels remain discernible [40]. We estimate a negligible upper bound of  $\langle N_T \rangle \approx 0.016$  for the average number of thermal atoms occupying each mode  $|\pm k\rangle_{\pm 1}$  (Methods), indicating that the observed distributions indeed arise from the amplification of quantum fluctuations with empty-mode occupations  $\langle N_{\text{QF}} \rangle \approx 0.5$ .

Going beyond studies of individual modes, we further verify the correlated nature of the produced pairs. We introduce the inter-spin noise correlation map

$$\mathcal{C}^{+1,-1}(k_{+1}^z, k_{-1}^z) = \frac{\langle n_{+1}n_{-1} \rangle - \langle n_{+1} \rangle \langle n_{-1} \rangle}{\sigma(n_{+1})\sigma(n_{-1})}, \quad (3)$$

with  $n_m \equiv n_m(k_m^z)$  indicating the momentum-space density distribution of spin state  $m$  along  $z$  (after integrating along  $x$ ) at coordinate  $k_m^z$ , and  $\sigma(n_m) = \langle n_m^2 \rangle - \langle n_m \rangle^2$ . In Figs. 2e and f, we show the extracted correlation maps

$\mathcal{C}^{+1,-1}(k_{+1}^z, k_{-1}^z)$  for both the single-channel and two-channel configurations, respectively. In the former case, we observe positive correlations around  $(k_{+1}^z, k_{-1}^z) = (+k, -k)$ , demonstrating that pairs occupy the modes  $|+k\rangle_{+1}$  and  $|-k\rangle_{-1}$  in a correlated fashion. For the latter case, the positive peaks around  $(+k, -k)$  and  $(-k, +k)$  indicate correlated generation of  $m = \pm 1$  pairs via the two channels  $\chi_{\pm}$ . When postselecting for realizations above a minimum pair number  $N_p^{\min}$ , we observe increasingly pronounced anticorrelation peaks for the two-channel configuration around equal momenta  $(+k, +k)$  and  $(-k, -k)$ , cf. Fig. 2g. We attribute this behaviour to the competition between the channels in the presence of pump-mode depletion, which inhibits large simultaneous occupation of these modes. This trend suggests that the many-body state cannot be merely expressed as a product state of two-mode squeezed vacuum states in the individual channels, especially in a regime of large occupations.

A deeper understanding of the pair dynamics and its interplay with depletion effects can be gained by investigating the full population evolution of the different modes (Fig. 3a). For clarity, we concentrate on the single-channel configuration involving the modes  $|+k\rangle_{+1}$  and  $|-k\rangle_{-1}$ . We observe the onset of pair production around  $T_{\text{int}} \approx 40 \mu\text{s}$ , followed by a fast exponential population increase; this behaviour is in resemblance to optical parametric amplification [5]. As time elapses, we observe coherent many-body oscillations redistributing the atoms between the different available modes. These pair oscillations are a consequence of the restricted phase space at finite  $N$ . While similar to pair oscillations arising from spin-mixing interactions [6], our observations also demonstrate coherent pair dynamics involving well-defined momentum modes.

For longer times, we observe a progressive accumulation of atoms in  $|+k\rangle_{+1}$  (see inset in Fig. 3a), resulting in a population imbalance between  $|+k\rangle_{+1}$  and  $|-k\rangle_{-1}$ . The oscillations are damped on a timescale  $T_{\text{coh}} \sim 150 \mu\text{s}$ , which we identify as the coherence time. We attribute both effects to the intrinsic open nature of our system as photons are sporadically lost at the cavity mirrors, inhibiting pair production through photon exchange. We model this dissipative superradiant Raman process via effective Lindblad terms with rates  $\gamma_{\pm} = \eta^2 \frac{2\kappa}{\delta_{\pm}^2 + \kappa^2}$  for the two channels, and perform truncated Wigner simulations (Methods), which stochastically sample quantum fluctuations of the initially empty modes in  $m = \pm 1$  [41]. Our simulations quantitatively reproduce the observed population evolution (solid lines in Fig. 3a), with the coupling  $\eta$  being the only free parameter of the simulations and optimized to  $\eta = 0.94\eta_{\text{exp}}$  of the experimentally calibrated value  $\eta_{\text{exp}}$ . We attribute this small difference to the imperfect alignment between the BEC and the cavity mode, and systematic uncertainties in the atom-number calibra-

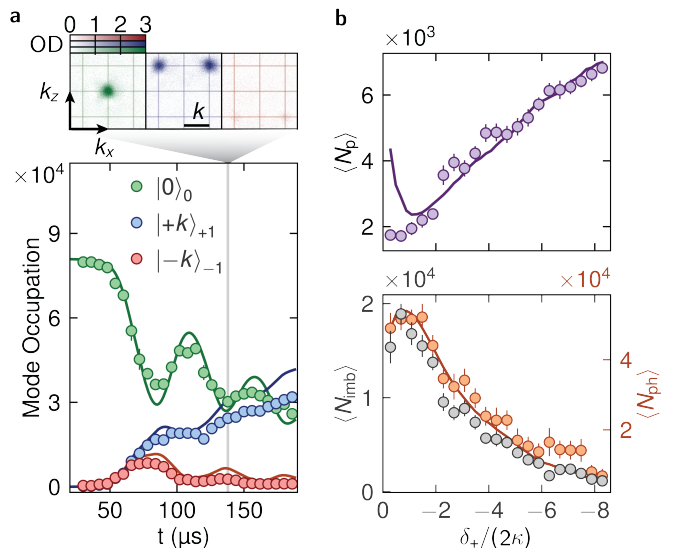


**FIG. 3. Coherent many-body oscillations and tunable dissipation.** **a**, Time evolution of mode occupations in the single-channel configuration, exhibiting oscillatory dynamics. The solid curves show numerical simulations (Methods). For longer times, photon loss results in an imbalance between the  $|+k\rangle_{+1}$  and  $|-k\rangle_{-1}$  populations. Inset: representative momentum-space distribution with large imbalance at  $t = 138 \mu\text{s}$ . **b**, Mean number of pairs  $\langle N_p \rangle$  (upper panel) and imbalance  $\langle N_{\text{imb}} \rangle$  (lower panel, grey), and number of photons lost from the cavity  $\langle N_{\text{ph}} \rangle$  (lower panel, orange) [38] for  $t = 80 \mu\text{s}$  as a function of the detuning  $\delta_+/(2\kappa)$ , which controls the coherent and dissipative processes. We attribute both the deviation from theory at large quench times as well as the excess photon numbers ( $\langle N_{\text{ph}} \rangle > \langle N_{\text{imb}} \rangle$ ) to superradiant decay to higher-order momentum modes in  $m = 1$ , which are outside the field of view ( $\sim 2.2k$ ) along  $x$  [38]. See Methods for all relevant experimental parameters.

tion. Note that the simulations also indicate that for our experimental parameters on average  $\sim \chi_+/\gamma_+ \approx 10$  pairs are created before the first photon is lost from the cavity.

Finally, the scaling of the couplings  $\chi_{\pm}/\gamma_{\pm} = \delta_{\pm}/(2\kappa)$  allows us to independently tune the coherent and dissipative processes of our system. We demonstrate this control for the single-channel configuration by quenching to a fixed coupling  $\chi_+ = -2\pi \times 0.61(3) \text{ Hz}$  and varying the detuning  $\delta_+$  at a constant  $t = 80 \mu\text{s}$ , see Fig. 3b. The measured mean number of pairs  $\langle N_p \rangle$  (upper panel) remains small close to the two-photon resonance ( $\delta_+ = 0$ ), and monotonically increases for large detunings  $|\delta_+|/(2\kappa) \gg 1$ . Concurrently, the mean population imbalance  $\langle N_{\text{imb}} \rangle$  between  $|+k\rangle_{+1}$  and  $|-k\rangle_{-1}$  (lower panel) exhibits the opposite trend and gradually decreases towards zero for large detunings. We also present the number of photons  $\langle N_{\text{ph}} \rangle$  lost from the cavity, as measured with our heterodyne detection [38]. The qualitative agreement between  $\langle N_{\text{ph}} \rangle$  and  $\langle N_{\text{imb}} \rangle$  verifies that superradiant Raman scattering is indeed the primary dissipative source. The experimental results are reasonably

captured by our numerical simulations. The deviation of the simulated pair number  $\langle N_p \rangle$  at  $|\delta_+|/(2\kappa) \lesssim 1$  is ascribed to the limited validity of the adiabatic elimination of the cavity field in this regime.

In conclusion, we experimentally demonstrate the creation of correlated atom pairs in well-defined spin and momentum modes via a superradiant photon-exchange process in a degenerate Bose gas. Our scheme amplifies vacuum fluctuations to induce fast photon-mediated spin-mixing dynamics within tens of microseconds. We demonstrate independent control over coherent and dissipative processes, and probe them by measurements of atomic and photonic observables. As the dynamics remains coherent for long times,  $T_{\text{coh}} \gg T_{\text{int}}$ , our results pave the way for fast entanglement generation in spatially separated atomic clouds [42, 43]. Combining such a mechanism with mode-selective spin rotations offers a promising route for performing loophole-free Bell tests with massive particles [44, 45]. As both the sign and strength of the photon-mediated interactions can be independently controlled, our system offers prospects for implementing time-reversal protocols for noise-resilient atom interferometry [46, 47]. Finally, extending our experimental scheme to degenerate Fermi gases could facilitate the manipulation of photon-induced Cooper pairs [48, 49].

---

\* These authors contributed equally to this work.

† [donner@phys.ethz.ch](mailto:donner@phys.ethz.ch)

- [1] S. W. Hawking, Black hole explosions?, *Nature* **248**, 30 (1974).
- [2] R. Bousso and S. W. Hawking, Pair creation of black holes during inflation, *Phys. Rev. D* **54**, 6312 (1996).
- [3] J. Bardeen, L. N. Cooper, and J. R. Schrieffer, Microscopic theory of superconductivity, *Phys. Rev.* **106**, 162 (1957).
- [4] J. M. Kosterlitz and D. J. Thouless, Ordering, metastability and phase transitions in two-dimensional systems, *J. Phys. C: Solid State Phys.* **6**, 1181 (1973).
- [5] R. W. Boyd, *Nonlinear Optics*, third edition ed. (Academic Press, Burlington, 2008).
- [6] M.-S. Chang, Q. Qin, W. Zhang, L. You, and M. S. Chapman, Coherent spinor dynamics in a spin-1 Bose condensate, *Nat. Phys.* **1**, 111 (2005).
- [7] C. Klempt, O. Topic, G. Gebreyesus, M. Scherer, T. Henninger, P. Hyllus, W. Ertmer, L. Santos, and J. J. Arlt, Parametric Amplification of Vacuum Fluctuations in a Spinor Condensate, *Phys. Rev. Lett.* **104**, 195303 (2010).
- [8] B. Lücke, M. Scherer, J. Kruse, L. Pezzé, F. Deuretzbacher, P. Hyllus, O. Topic, J. Peise, W. Ertmer, J. Arlt, L. Santos, A. Smerzi, and C. Klempt, Twin Matter Waves for Interferometry Beyond the Classical Limit, *Science* **334**, 773 (2011).
- [9] E. M. Bookjans, C. D. Hamley, and M. S. Chapman, Strong Quantum Spin Correlations Observed in Atomic Spin Mixing, *Phys. Rev. Lett.* **107**, 210406 (2011).
- [10] C. Gross, H. Strobel, E. Nicklas, T. Zibold, N. Bar-Gill, G. Kurizki, and M. K. Oberthaler, Atomic homodyne detection of continuous-variable entangled twin-atom states, *Nature* **480**, 219 (2011).
- [11] A. Qu, B. Evrard, J. Dalibard, and F. Gerbier, Probing Spin Correlations in a Bose-Einstein Condensate Near the Single-Atom Level, *Phys. Rev. Lett.* **125**, 033401 (2020).
- [12] D. K. Shin, B. M. Henson, S. S. Hodgman, T. Wasak, J. Chwedeńczuk, and A. G. Truscott, Bell correlations between spatially separated pairs of atoms, *Nat. Commun.* **10**, 4447 (2019).
- [13] L. Deng, E. W. Hagley, J. Wen, M. Trippenbach, Y. Band, P. S. Julienne, J. E. Simsarian, K. Helmerston, S. L. Rolston, and W. D. Phillips, Four-wave mixing with matter waves, *Nature* **398**, 218 (1999).
- [14] J. M. Vogels, K. Xu, and W. Ketterle, Generation of Macroscopic Pair-Correlated Atomic Beams by Four-Wave Mixing in Bose-Einstein Condensates, *Phys. Rev. Lett.* **89**, 020401 (2002).
- [15] N. Gemelke, E. Sarajlic, Y. Bidel, S. Hong, and S. Chu, Parametric Amplification of Matter Waves in Periodically Translated Optical Lattices, *Phys. Rev. Lett.* **95**, 170404 (2005).
- [16] G. K. Campbell, J. Mun, M. Boyd, E. W. Streed, W. Ketterle, and D. E. Pritchard, Parametric Amplification of Scattered Atom Pairs, *Phys. Rev. Lett.* **96**, 020406 (2006).
- [17] A. Perrin, H. Chang, V. Krachmalnicoff, M. Schellekens, D. Boiron, A. Aspect, and C. I. Westbrook, Observation of Atom Pairs in Spontaneous Four-Wave Mixing of Two Colliding Bose-Einstein Condensates, *Phys. Rev. Lett.* **99**, 150405 (2007).
- [18] R. G. Dall, L. J. Byron, A. G. Truscott, G. R. Dennis, M. T. Johnsson, and J. J. Hope, Paired-atom laser beams created via four-wave mixing, *Phys. Rev. A* **79**, 011601 (2009).
- [19] V. Krachmalnicoff, J.-C. Jaskula, M. Bonneau, V. Leung, G. B. Partridge, D. Boiron, C. I. Westbrook, P. Deuar, P. Ziñ, M. Trippenbach, and K. V. Kheruntsyan, Spontaneous four-wave mixing of de broglie waves: Beyond optics, *Phys. Rev. Lett.* **104**, 150402 (2010).
- [20] D. Pertot, B. Gadway, and D. Schneble, Collinear Four-Wave Mixing of Two-Component Matter Waves, *Phys. Rev. Lett.* **104**, 200402 (2010).
- [21] R. Bücker, J. Grond, S. Manz, T. Berrada, T. Betz, C. Koller, U. Hohenester, T. Schumm, A. Perrin, and J. Schmiedmayer, Twin-atom beams, *Nat. Phys.* **7**, 608 (2011).
- [22] M. Bonneau, J. Ruaudel, R. Lopes, J.-C. Jaskula, A. Aspect, D. Boiron, and C. I. Westbrook, Tunable source of correlated atom beams, *Phys. Rev. A* **87**, 061603 (2013).
- [23] S. Hodgman, R. Khakimov, R. Lewis-Swan, A. Truscott, and K. Kheruntsyan, Solving the Quantum Many-Body Problem via Correlations Measured with a Momentum Microscope, *Phys. Rev. Lett.* **118**, 240402 (2017).
- [24] L. W. Clark, A. Gaj, L. Feng, and C. Chin, Collective emission of matter-wave jets from driven Bose-Einstein condensates, *Nature* **551**, 356 (2017).
- [25] F. Anders, A. Idel, P. Feldmann, D. Bondarenko, S. Loriani, K. Lange, J. Peise, M. Gersemann, B. Meyer-Hoppe, S. Abend, N. Gaaloul, C. Schubert, D. Schlippert, L. Santos, E. Rasel, and C. Klempt, Momentum Entanglement for Atom Interferometry, *Phys. Rev. Lett.* **127**, 140402 (2021).

- [26] L. Pezzè, A. Smerzi, M. K. Oberthaler, R. Schmied, and P. Treutlein, Quantum metrology with nonclassical states of atomic ensembles, *Rev. Mod. Phys.* **90**, 035005 (2018).
- [27] S. S. Szigeti, O. Hosten, and S. A. Haine, Improving cold-atom sensors with quantum entanglement: Prospects and challenges, *Appl. Phys. Lett.* **118**, 140501 (2021).
- [28] S. Inouye, A. P. Chikkatur, D. M. Stamper-Kurn, J. Stenger, D. E. Pritchard, and W. Ketterle, Superradiant Rayleigh Scattering from a Bose-Einstein Condensate, *Science* **285**, 571 (1999).
- [29] E. Hagley, X. Maitre, G. Nogues, C. Wunderlich, M. Brune, J. M. Raimond, and S. Haroche, Generation of Einstein-Podolsky-Rosen Pairs of Atoms, *Phys. Rev. Lett.* **79**, 1 (1997).
- [30] E. J. Davis, G. Bentsen, L. Homeier, T. Li, and M. H. Schleier-Smith, Photon-Mediated Spin-Exchange Dynamics of Spin-1 Atoms, *Phys. Rev. Lett.* **122**, 010405 (2019).
- [31] E. J. Davis, A. Periwal, E. S. Cooper, G. Bentsen, S. J. Evered, K. Van Kirk, and M. H. Schleier-Smith, Protecting Spin Coherence in a Tunable Heisenberg Model, *Phys. Rev. Lett.* **125**, 060402 (2020).
- [32] A. Periwal, E. S. Cooper, P. Kunkel, J. F. Wienand, E. J. Davis, and M. Schleier-Smith, Programmable interactions and emergent geometry in an array of atom clouds, *Nature* **600**, 630 (2021).
- [33] K. Kim, J. Hur, S. Huh, S. Choi, and J.-y. Choi, Emission of Spin-Correlated Matter-Wave Jets from Spinor Bose-Einstein Condensates, *Phys. Rev. Lett.* **127**, 043401 (2021).
- [34] T. Weber, J. Herbig, M. Mark, H.-C. Nägerl, and R. Grimm, Three-Body Recombination at Large Scattering Lengths in an Ultracold Atomic Gas, *Phys. Rev. Lett.* **91**, 123201 (2003).
- [35] R. Grimm, M. Weidemüller, and Y. B. Ovchinnikov, Optical Dipole Traps for Neutral Atoms, *Adv. At. Mol. Opt.* **42**, 95 (2000).
- [36] G. Vrijsen, O. Hosten, J. Lee, S. Bernon, and M. A. Kasevich, Raman Lasing with a Cold Atom Gain Medium in a High-Finesse Optical Cavity, *Phys. Rev. Lett.* **107**, 063904 (2011).
- [37] J. G. Bohnet, Z. Chen, J. M. Weiner, D. Meiser, M. J. Holland, and J. K. Thompson, A steady-state superradiant laser with less than one intracavity photon, *Nature* **484**, 78 (2012).
- [38] R. Rosa-Medina, F. Ferri, F. Finger, N. Dogra, K. Kroeger, R. Lin, R. Chitra, T. Donner, and T. Esslinger, Observing Dynamical Currents in a Non-Hermitian Momentum Lattice, *Phys. Rev. Lett.* **128**, 143602 (2022).
- [39] B. Yurke and M. Potasek, Obtainment of thermal noise from a pure quantum state, *Phys. Rev. A* **36**, 3464 (1987).
- [40] F. Paleari, A. Andreoni, G. Zambra, and M. Bondani, Thermal photon statistics in spontaneous parametric downconversion, *Opt. Express* **12**, 2816 (2004).
- [41] P. B. Blakie, A. S. Bradley, M. J. Davis, R. J. Ballagh, and C. W. Gardiner, Dynamics and statistical mechanics of ultra-cold Bose gases using c-field techniques, *Adv. Phys.* **57**, 363 (2008).
- [42] L. Salvi, N. Poli, V. Vuletić, and G. M. Tino, Squeezing on Momentum States for Atom Interferometry, *Phys. Rev. Lett.* **120**, 033601 (2018).
- [43] G. P. Greve, C. Luo, B. Wu, and J. K. Thompson, Entanglement-enhanced matter-wave interferometry in a high-finesse cavity, *Nature* **610**, 472 (2022).
- [44] R. J. Lewis-Swan and K. V. Kheruntsyan, Proposal for a motional-state Bell inequality test with ultracold atoms, *Phys. Rev. A* **91**, 052114 (2015).
- [45] J. Kitzinger, X. Meng, M. Fadel, V. Ivannikov, K. Nemoto, W. J. Munro, and T. Byrnes, Bell correlations in a split two-mode-squeezed Bose-Einstein condensate, *Phys. Rev. A* **104**, 043323 (2021).
- [46] D. Linnemann, H. Strobel, W. Muessel, J. Schulz, R. Lewis-Swan, K. Kheruntsyan, and M. Oberthaler, Quantum-Enhanced Sensing Based on Time Reversal of Nonlinear Dynamics, *Phys. Rev. Lett.* **117**, 013001 (2016).
- [47] S. Colombo, E. Pedrozo-Peñafiel, A. F. Adiyatullin, Z. Li, E. Mendez, C. Shu, and V. Vuletić, Time-reversal-based quantum metrology with many-body entangled states, *Nat. Phys.* **18**, 925 (2022).
- [48] E. Colella, R. Citro, M. Barsanti, D. Rossini, and M.-L. Chiofalo, Quantum phases of spinful fermi gases in optical cavities, *Phys. Rev. B* **97**, 134502 (2018).
- [49] R. J. Lewis-Swan, D. Barberena, J. R. K. Cline, D. J. Young, J. K. Thompson, and A. M. Rey, Cavity-QED Quantum Simulator of Dynamical Phases of a Bardeen-Cooper-Schrieffer Superconductor, *Phys. Rev. Lett.* **126**, 173601 (2021).
- [50] F. Schmidt, D. Mayer, M. Hohmann, T. Lausch, F. Kindermann, and A. Widera, Precision measurement of the  $^{87}\text{Rb}$  tune-out wavelength in the hyperfine ground state  $f = 1$  at 790 nm, *Phys. Rev. A* **93**, 022507 (2016).
- [51] M. Landini, N. Dogra, K. Kroeger, L. Hruby, T. Donner, and T. Esslinger, Formation of a Spin Texture in a Quantum Gas Coupled to a Cavity, *Phys. Rev. Lett.* **120**, 223602 (2018).
- [52] B. Gadway, D. Pertot, R. Reimann, M. G. Cohen, and D. Schneble, Analysis of Kapitza-Dirac diffraction patterns beyond the Raman-Nath regime, *Opt. Express* **17**, 19173 (2009).
- [53] F. Ferri, R. Rosa-Medina, F. Finger, N. Dogra, M. Soriante, O. Zilberberg, T. Donner, and T. Esslinger, Emerging Dissipative Phases in a Superradiant Quantum Gas with Tunable Decay, *Phys. Rev. X* **11**, 041046 (2021).
- [54] R. J. Fletcher, M. Robert-de Saint-Vincent, J. Man, N. Navon, R. P. Smith, K. G. H. Viebahn, and Z. Hadzibabic, Connecting Berezinskii-Kosterlitz-Thouless and BEC Phase Transitions by Tuning Interactions in a Trapped Gas, *Phys. Rev. Lett.* **114**, 255302 (2015).
- [55] F. Brennecke, S. Ritter, T. Donner, and T. Esslinger, Cavity Optomechanics with a Bose-Einstein Condensate, *Science* **322**, 235 (2008).
- [56] F. Reiter and A. S. Sørensen, Effective operator formalism for open quantum systems, *Phys. Rev. A* **85**, 032111 (2012).

**Acknowledgments.** We are grateful to Alexander Frank for his contributions to the electronic setup of the experiment, and to Florentin Reiter, Davide Dreon, and Meng-Zi Huang for fruitful discussions. We thank Jean-Philippe Brantut for carefully reading the manuscript. We acknowledge funding from the Swiss National Science Foundation: project numbers 200020\_212168 and 20QT-1.205584 and NCCR QSIT (Grant No. 51NF40-185902),

and from EU Horizon2020: ERC advanced grant TransQ (project Number 742579).

**Author contributions.** F.F., R.R., N.R. and P.C. prepared the experiment, collected, and analysed the experimental data, and formulated the theory framework. T.D. and T.E. supervised the work. All authors contributed to the preparation and discussion of the manuscript.

**Competing interests.** The authors declare no competing interests.

## METHODS

**Experimental details.** We operate the drive laser at 790.019 nm, i.e., the  $^{87}\text{Rb}$  D-line tune-out wavelength [50], where the scalar ac-Stark shift vanishes for  $F = 1$ . This suppresses spurious potentials and minimizes spontaneous emission, otherwise relevant for the operating powers  $\sim 100$  mW. We experimentally verify that the drive does not induce significant losses by monitoring the atom-number evolution while illuminating with the maximum experimentally used laser power. The measured  $1/e$  lifetime of 47(7) ms is orders of magnitude larger than our relevant experimental timescales of  $\sim 100$   $\mu\text{s}$ . Note that during this measurement we keep the cavity unlocked to avoid cavity-induced interactions. The drive polarization is chosen along  $y$  to inhibit atomic self-organization in the  $m = \pm 1$  sublevels mediated by the vectorial polarizability [51].

In Table I, we list all relevant experimental parameters for the measurements shown in this work. For the measurements of Fig. 3(b-c), we adjust the drive power  $P$  and thus  $\eta \propto \sqrt{P}$  to keep  $\chi_+ = -2\pi \times 0.64(1)$  Hz constant. We calibrate  $P$  using Kapitza-Dirac diffraction [52]. Following Refs. [38, 53], we tune the drive away from the tune-out wavelength and illuminate the atoms in a standing-wave configuration.

Fig. $N(\times 10^4)$	$t(\mu\text{s})$	$\omega_z/2\pi$ (MHz)	$\delta_+/2\pi$ (MHz)	$\chi_+/2\pi$ (Hz)
1c	65	7.09(1)	-20.7(3)	-0.64(1)
2a,c	4.0(3)	60	7.09(1)	-18.7(3)
2b,d	5.3(4)	62	1.01(1)	-18.7(3)
2e	7.2(6)	62	7.09(1)	-25.7(3)
2f	7.0(6)	62	0.90(1)	-25.7(1)
3a	8.1(3)		7.09(1)	-22.7(1)
3b,c	7.9(3)	80	7.09(1)	-0.64(1)

TABLE I. List of experimental parameters.

**Detection and calibration of atom populations.** We measure the momentum distribution by shining a

high-intensity imaging beam along  $y$  on the atoms after 5.5–6.2 ms of time-of-flight (TOF) expansion. To spatially resolve atoms in the different  $m$  sublevels, we apply a magnetic field gradient along  $z$  during TOF (Stern-Gerlach separation). We extract the atom populations in the different spin and momentum states from circular-shaped crops in the absorption images. For that, we correct for short-scale intensity variations in the imaging-beam profile [54]. Such variations mainly originate from diffraction effects on the cavity which acts as a thick slit for the light. Our detection is finally calibrated with a systematic uncertainty of  $\sim 15\%$  using the dispersive shift of the cavity resonance in the presence of a  $m = 0$  BEC [55]. We additionally verify the absence of significant  $m$ -dependent effects on atom counting. To do so, we drive an initially polarized BEC in  $m = -1$  in a three-level Rabi oscillation and observe a constant total atom number while the populations of the three  $m$  states change.

The technical detection noise in our system is well captured by a Gaussian distribution [10] as shown by the fit in Fig. 2c (right panel), yielding a standard deviation of  $\sigma_{\text{det}} \approx 200$ . The distributions are then fit by a convolution of a Bose-Einstein distribution  $p(N_p, \langle N_p \rangle)$  and a normalized Gaussian  $G(N_p, \sigma_G, \mu)$

$$P(N_p, \langle N_p \rangle, \sigma_G, \mu) = p(N_p, \langle N_p \rangle) * G(N_p, \sigma_G, \mu), \quad (4)$$

where  $\langle N_p \rangle$  is the mean pair number extracted from the raw distribution and  $\sigma_G$  and  $\mu$  remain fit parameters to capture position-dependent noise effects; we find  $\sigma_G \approx \sigma_{\text{det}}$ . Assuming uncorrelated physical and technical fluctuations, we estimate the standard deviation of the pair histograms as  $\sigma(N_p) = \sqrt{\sigma_{\text{exp}}^2(N_p) - \sigma_G^2}$ , where  $\sigma_{\text{exp}}(N_p)$  is the experimentally measured standard deviation.

**Experimental timescales.** The timescale to produce pairs,  $T_{\text{int}} = 2\pi / (N \max|\chi_{\pm}^{\text{eff}}|)$ , is determined by the collective couplings  $N\chi_{\pm}$ . For typical values of  $N \approx 8 \times 10^4$  and  $\chi_+^{\text{eff}} = (\eta/\eta_{\text{exp}})^2 \chi_+$ , we obtain  $T_{\text{int}} \approx 40$   $\mu\text{s}$ . On the other hand, the lifetime of the pairs is limited by the harmonic trapping potential since the paired states with  $\pm \hbar k$  are not its eigenstates. We estimate the lifetime as  $T_{\text{LT}} = \min(T_{\text{exp}}, T_{\text{sep}})$  [23], with  $T_{\text{exp}} = 2\pi / \max(\omega_x, \omega_z)$  and  $T_{\text{sep}} = R_{\text{TF}}/v_{\text{rec}}$  being the characteristic timescales for the expansion in the harmonic trap and for the separation between the pairs and the zero-momentum BEC, respectively. Using the trap frequencies  $[\omega_x, \omega_y, \omega_z] = 2\pi \times [204(3), 34(2), 185(1)]$  Hz, the recoil velocity  $v_{\text{rec}} = 0.0058$  m/s and a Thomas-Fermi radius of  $R_{\text{TF}} \approx 5.8$   $\mu\text{m}$ , we obtain  $T_{\text{exp}} \approx 5$  ms and  $T_{\text{LT}} = T_{\text{sep}} \approx 1$  ms. The separation of timescales, quantified as  $T_{\text{LT}}/T_{\text{int}} \approx 25$  and  $T_{\text{LT}}/T_{\text{coh}} \approx 6.7$ , ensures that pairs are produced in well-defined individual momentum modes and remain in such throughout the entire dynamics. For comparison, collisionally induced pairs in metastable Helium BECs ex-

hibit a ratio of  $T_{\text{LT}}/T_{\text{int}} = 0.7$  [23], while for Floquet-engineered systems  $T_{\text{LT}}/T_{\text{int}} \lesssim 3$  [24]. Notably, these experiments operate in the spontaneous and weak collective regimes for pair production, respectively.

**Thermal occupation of the paired modes.** We estimate an upper bound for the thermal occupation of the individual modes that constitute the pairs and conclude that it is negligible compared to quantum fluctuations ( $\mathcal{O}(1)$ ). In our system, with  $N \approx 8 \times 10^4$  and a mean trap frequency  $\bar{\omega} = (\omega_x \omega_y \omega_z)^{1/3} = 2\pi \times 109$  Hz, we get a critical temperature  $T_c \approx 210$  nK, and thus a realistic estimation for the cloud's temperature  $T \lesssim 100$  nK for a condensate fraction of  $N_c/N \gtrsim 0.9$  [55]. Due to a Thomas-Fermi density profile, the momentum-space spread of the initial BEC and the produced modes is  $\delta k = 2\pi/R_{\text{TF}} \approx 0.12k$ , in agreement with our absorption images. Taking into account the width  $\delta k$  of the paired modes, the probability to thermally occupy each of them is

$$P = 2 \int_{k-\delta k}^{k+\delta k} \int_{-\delta k}^{\delta k} \int_{k-\delta k}^{k+\delta k} p(\mathbf{k}, T) dk_x dk_y dk_z \approx 2.8 \times 10^{-4} \quad (5)$$

for  $T = 100$  nK, where  $p(\mathbf{k}, T) = \mathcal{N} \left[ \exp\left(\frac{E(\mathbf{k})}{k_B T}\right) + 1 \right]^{-1}$  is the momentum-space probability distribution for the thermal  $^{87}\text{Rb}$  atoms of mass  $M$ . Here  $E(\mathbf{k}) = \hbar^2 \mathbf{k}^2 / (2M)$  is the kinetic energy associated with the momenta  $\hbar \mathbf{k} = \hbar(k_x, k_y, k_z)$ ,  $k_B$  the Boltzmann constant and  $\mathcal{N}$  a suitable normalization factor. In our experiment, we prepare a BEC solely in  $m = 0$  as the initial step for the generation of pairs by applying a strong magnetic-field gradient to clean spurious atoms in  $m = \pm 1$  [51]. From our detection, we can safely assume that the population  $N_{\pm 1}$  of these sublevels is  $< 3\sigma_{\text{det}}$ , which lies within the 99.7% confidence interval of our detection, and thus a total number of thermal atoms in  $m = \pm 1$  of  $N_{\pm 1}^T < (N - N_c)/N \times 3\sigma_{\text{det}} = 60$ . The average number of thermal atoms occupying the modes  $|\pm k\rangle_{\pm 1}$  is then  $\langle N_T \rangle = P N_{\pm 1}^T < 0.016 \ll \mathcal{O}(1)$ .

**Derivation of the many-body Hamiltonian.** The Hamiltonian of a single atom dispersively coupled to a single cavity mode by a running-wave laser drive is

$$\begin{aligned} \hat{H}_{\text{SP}} &= \frac{\hat{p}^2}{2M} + \hbar\omega_z \hat{F}_z + \hbar q \hat{F}_z^2 + \hbar\omega_c \hat{a}^\dagger \hat{a} \\ &\quad - i \frac{\alpha_v}{2F} \left[ \hat{\mathbf{E}}^{(+)} \times \hat{\mathbf{E}}^{(-)} \right] \cdot \hat{\mathbf{F}}. \end{aligned} \quad (6)$$

Here, the first term denotes the kinetic energy of the atom,  $\omega_z/B = -2\pi \times 700$  kHz/G and  $q/B^2 = 2\pi \times 72$  Hz/G<sup>2</sup> are the linear and quadratic Zeeman splittings, and  $\hat{\mathbf{F}} = (\hat{F}_x, \hat{F}_y, \hat{F}_z)^T$  is the spin operator for the  $F = 1$  manifold. The operator  $\hat{a}^\dagger$  creates a photon in the  $z$ -polarized cavity mode of frequency  $\omega_c$ . Because of our

choice of drive wavelength, we consider atom-light interactions mediated only by the vectorial polarizability  $\alpha_v$ . The cavity mode extends along  $x$  and has a field amplitude  $E_0 = 403$  V/m per photon [53]. With  $E_d$  indicating the amplitude of the drive with frequency  $\omega_d$  propagating along  $+z$ , the negative part of the total electric field is represented by

$$\hat{\mathbf{E}}^{(-)} = \frac{E_d}{2} e^{ikz} e^{-i\omega_d t} \mathbf{e}_y + E_0 \cos(kx) \hat{a} \mathbf{e}_z, \quad (7)$$

with unit vectors  $\mathbf{e}_j$ ,  $j \in \{x, y, z\}$ . A unitary transformation  $\hat{U} = e^{i\hat{H}_{\text{rot}} t/\hbar}$  with  $\hat{H}_{\text{rot}} = \hbar\omega_d \hat{a}^\dagger \hat{a} + \hbar\omega_z \hat{F}_z$ , and a global phase rotation  $\hat{a} \rightarrow \hat{a} e^{i\pi/2}$  gives

$$\begin{aligned} \hat{H}_{\text{SP}} &= \frac{\hat{p}^2}{2M} - \hbar\delta_c \hat{a}^\dagger \hat{a} + \hbar q \hat{F}_z^2 \\ &\quad + \frac{\alpha_v E_0 E_d \cos(kx)}{8} \left[ (\hat{a}^\dagger e^{ikz} - \hat{a} e^{-ikz}) (\hat{F}_+ e^{i\omega_z t} + \hat{F}_- e^{-i\omega_z t}) \right], \end{aligned} \quad (8)$$

with a drive-cavity detuning  $\delta_c = \omega_d - \omega_c$ . Note that  $|\delta_c| < 2\pi \times 10$  MHz is small compared to the frequency of the drive, and thus we assume a common wavenumber  $k$  for the drive and the cavity.

We derive the many-body Hamiltonian using a six-mode expansion in momentum- and spin-space. The selected modes comprise  $|0\rangle_0$ , with a single-particle wavefunction  $\psi \propto 1$ , the four modes  $|\pm k\rangle_{\pm 1}$  occupied by pairs, with  $\psi \propto \cos(kx) e^{(\pm)ikz}$ , and the next-order mode  $\{k_x, k_z, m\} = \{\pm 2k, 0, 0\} \equiv |\pm 2k\rangle_0$ , with  $\psi \propto \cos^2(kx)$ . The latter participates due to the interaction between pairs in  $m = \pm 1$ . The corresponding spinor field operator is

$$\begin{aligned} \hat{\Psi}(\mathbf{x}) &= \left( \hat{\Psi}_{+1}(\mathbf{x}), \hat{\Psi}_0(\mathbf{x}), \hat{\Psi}_{-1}(\mathbf{x}) \right)^T \\ &= \begin{pmatrix} \frac{k}{\sqrt{2\pi}} \cos(kx) (e^{ikz} \hat{c}_{k,+1} + e^{-ikz} \hat{c}_{-k,+1}) \\ \frac{k}{2\pi} \hat{c}_{0,0} + \frac{\sqrt{2}k}{\sqrt{3\pi}} \cos^2(kx) \hat{c}_{0,\pm 2k_x} \\ \frac{k}{\sqrt{2\pi}} \cos(kx) (e^{-ikz} \hat{c}_{-k,-1} + e^{ikz} \hat{c}_{+k,-1}) \end{pmatrix}, \end{aligned} \quad (9)$$

where the operators  $\hat{c}_{\vec{k},m}$  follow the main-text definitions. If the two-photon detunings  $\delta_{\pm} = -\delta_c \mp \omega_z = \omega_c - (\omega_d \pm \omega_z) = \omega_c - \omega_{\pm}$  significantly exceed the decay rate  $\kappa$ , superradiant Raman scattering from  $m = 0$  to  $m = \pm 1$  is suppressed. We adiabatically eliminate the cavity field following the formalism of Ref. [56] and

obtain the effective many-body Hamiltonian

$$\begin{aligned}
\hat{H} &= \hat{H}_0 + \hat{H}_+ + \hat{H}_-, \quad \text{with} \\
\hat{H}_0 &= \hbar \frac{\omega_0}{2} (\hat{c}_{+k,+1}^\dagger \hat{c}_{+k,+1} + \hat{c}_{-k,+1}^\dagger \hat{c}_{-k,+1} \\
&\quad + \hat{c}_{-k,-1}^\dagger \hat{c}_{-k,-1} + \hat{c}_{+k,-1}^\dagger \hat{c}_{+k,-1}) \\
&\quad + 4\hbar\omega_{\text{rec}} \hat{c}_{0,\pm 2k_x}^\dagger \hat{c}_{0,\pm 2k_x}, \\
\hat{H}_+ &= \hbar\chi_+ (2\hat{c}_{-k,-1}^\dagger \hat{c}_{+k,+1}^\dagger \hat{c}_0 \hat{c}_0 + \hat{c}_0^\dagger \hat{c}_{+k,+1} \hat{c}_{+k,+1}^\dagger \hat{c}_0) \quad (10) \\
&\quad + \hat{c}_{-k,-1}^\dagger \hat{c}_0 \hat{c}_0^\dagger \hat{c}_{-k,-1} + \text{h.c.}), \\
\hat{H}_- &= \hbar\chi_- (2\hat{c}_{-k,+1}^\dagger \hat{c}_{+k,-1}^\dagger \hat{c}_0 \hat{c}_0 + \hat{c}_0^\dagger \hat{c}_{-k,+1} \hat{c}_{-k,+1}^\dagger \hat{c}_0 \\
&\quad + \hat{c}_0^\dagger \hat{c}_{+k,-1} \hat{c}_{+k,-1}^\dagger \hat{c}_0 + \text{h.c.}),
\end{aligned}$$

where we additionally use the notation  $\hat{c}_0 = (\hat{c}_{0,0} + \sqrt{\frac{2}{3}}\hat{c}_{0,\pm 2k_x})$ . The four-photon coupling rates, given in the main text, depend on the two-photon Raman couplings  $\eta = \beta\alpha_v E_0 E_d / 8\hbar$ . The factor  $\beta \approx 0.91$  arises from the overlap integrals between the harmonically confined atomic cloud, the cavity mode and the drive [53]. In the  $\hat{H}_\pm$  terms, the first part describes the production of pairs in  $m = \pm 1$  starting from  $m = 0$ , while the second (third) describes spin-exchange interactions between  $m = 0 \leftrightarrow m = 1$  ( $m = 0 \leftrightarrow m = -1$ ). In presenting the Hamiltonian Eq. (2) in the main text we omit the latter parts, as spin-exchange dynamics is suppressed when the majority of the atoms populate the pump mode. In the simulations, however, we take into account the full Hamiltonian.

**Dissipation.** The leakage of the cavity field makes our experiment intrinsically an open quantum system. We identify effective Lindblad terms

$$\hat{L}_\pm = \sqrt{\gamma_\pm} \left( \hat{c}_{+k,\pm 1}^\dagger \hat{c}_0 + \hat{c}_0^\dagger \hat{c}_{-k,\mp 1} \right), \quad (11)$$

which we derive within the framework of the effective operator formalism [56]. The term  $\hat{L}_\pm$  describes a superradiant Raman decay process, where atoms scatter photons into the cavity while changing their spin state  $m \rightarrow m \pm 1$  and obtaining net recoil momentum  $+\hbar k$  along  $z$ . These cavity photons get lost before they can be further rescattered. The dynamics of the open quantum system is determined by the master equation

$$\frac{d\hat{\rho}}{dt} = -\frac{i}{\hbar} [\hat{H}, \hat{\rho}] + \sum_{j \in \{+, -\}} \hat{L}_j \hat{\rho} \hat{L}_j^\dagger - \frac{1}{2} \left( \hat{L}_j^\dagger \hat{L}_j \hat{\rho} + \hat{\rho} \hat{L}_j^\dagger \hat{L}_j \right). \quad (12)$$

We define the normalized complex-valued expectation values  $\psi_{\vec{k},m} = \langle \hat{c}_{\vec{k},m} \rangle / \sqrt{N}$  for the different modes and derive mean-field equations of motion (EOM)

$$\begin{aligned}
\frac{d}{dt} \psi_{0,0} &= N [-i\chi_+ (2\psi_0^* \psi_{-k,-1} \psi_{k,1} + \psi_{k,1}^* \psi_0 \psi_{k,1} + \psi_{-k,-1}^* \psi_0 \psi_{-k,-1}) \\
&\quad - i\chi_- (2\psi_0^* \psi_{k,-1} \psi_{-k,1} + \psi_{-k,1}^* \psi_0 \psi_{-k,1} + \psi_{k,-1} \psi_0 \psi_{k,-1}^*) \\
&\quad + \gamma_+ (\psi_{k,1}^* \psi_{k,1} \psi_0 - \psi_{-k,-1}^* \psi_{-k,-1} \psi_0) \\
&\quad + \gamma_- (\psi_{-k,-1}^* \psi_{-k,-1} \psi_0 - \psi_{k,1}^* \psi_{k,1} \psi_0)] \\
\frac{d}{dt} \psi_{\pm k, \pm 1} &= -i \frac{\omega_0}{2} \psi_{\pm k, \pm 1} \\
&\quad \pm N (\gamma_+ \mp i\chi_+) (\psi_0^* \psi_0 \psi_{\pm k, \pm 1} + \psi_{\mp k, \mp 1}^* \psi_0 \psi_0) \\
\frac{d}{dt} \psi_{\mp k, \pm 1} &= -i \frac{\omega_0}{2} \psi_{\mp k, \pm 1} \\
&\quad \pm N (\gamma_- \mp i\chi_-) (\psi_0^* \psi_0 \psi_{\mp k, \pm 1} + \psi_{\pm k, \mp 1}^* \psi_0 \psi_0) \\
\frac{d}{dt} \psi_{\pm 2k_x, 0} &= -4i\omega_{\text{rec}} \psi_{\pm 2k_x, 0} \\
&+ \sqrt{\frac{2}{3}} N [-i\chi_+ (2\psi_0^* \psi_{-k,-1} \psi_{k,1} + \psi_{k,1}^* \psi_0 \psi_{k,1} + \psi_{-k,-1}^* \psi_0 \psi_{-k,-1}) \\
&\quad - i\chi_- (2\psi_0^* \psi_{k,-1} \psi_{-k,1} + \psi_{-k,1}^* \psi_0 \psi_{-k,1} + \psi_{k,-1} \psi_0 \psi_{k,-1}^*) \\
&\quad + \gamma_+ (\psi_{-k,-1}^* \psi_0 \psi_{-k,-1} - \psi_{k,1} \psi_0 \psi_{k,1}^*) \\
&\quad + \gamma_- (\psi_{-k,1}^* \psi_0 \psi_{-k,1} - \psi_{k,-1} \psi_0 \psi_{k,-1}^*)]. \quad (13)
\end{aligned}$$

**Simulations.** We model the dynamics in our system employing truncated Wigner simulations [41], which account for both quantum and experimental fluctuations. This method is used to simulate the fluctuations of spin-mixing dynamics in Bose-Einstein condensates satisfying the single spatial-mode approximation [46]. We initialize all the atoms in the mode  $\hat{c}_{0,0}$  by setting  $\psi_{0,0}(t=0) = 1$ , and sample all the other modes from complex-valued normal distributions with  $\mu = 0$  and  $\sigma^2 = 0.5$ . The latter is typically referred to as *quantum one-half noise* and models the quantum fluctuations of a coherent spin state. Practically, we sample 500 different initial conditions for the mean-field EOM in Eq. (13), which we then numerically evolve using built-in MATLAB methods. We also incorporate shot-to-shot fluctuations of the initial atom number, on the order of  $\Delta N/N = 0.05$ . We sample the atom number for each simulation from a Gaussian distribution with mean  $N$  and standard deviation  $\sigma(N) = 0.05N$ . Finally, we estimate the expectation value  $\langle \hat{O}(t) \rangle$  and the variance  $\sigma^2[\hat{O}(t)]$  of the observable  $\hat{O}(t)$  at any given time  $t$  by averaging over the different samples.